NASA TECHNICAL NOTE

NASA TN D-4953

NASA TN D-4953

PROJECTILE SHAPE EFFECTS ON HYPERVELOCITY IMPACT CRATERS IN ALUMINUM

by B. Pat Denardo

Ames Research Center
Moffett Field, Calif.

NATIONAL AERONAUTICS AND SPACE ADMINISTRATION • WASHINGTON, D. C. • DECEMBER 1968

NASA TN D-4953

PROJECTILE SHAPE EFFECTS ON HYPERVELOCITY IMPACT CRATERS IN ALUMINUM

By B. Pat Denardo

Ames Research Center
Moffett Field, Calif.

NATIONAL AERONAUTICS AND SPACE ADMINISTRATION

For sale by the Clearinghouse for Federal Scientific and Technical Information
Springfield, Virginia 22151 – CFSTI price $3.00

Page Intentionally Left Blank

PROJECTILE SHAPE EFFECTS ON HYPERVELOCITY IMPACT CRATERS IN ALUMINUM

By B. Pat Denardo

Ames Research Center

SUMMARY

Linear high-density polyethylene cylinders, with fineness ratios of 1/6, 1/3, 2/3, 1, and 3, and spheres were launched into thick targets of hard (2024-T351) aluminum at velocities up to 11.3 km/sec.

The effects of projectile shape on the various crater parameters were determined quantitatively from the basic crater dimensions: depth, diameter, and volume. In the hypervelocity regime, the dimensionless penetration, P/d, varied with the projectile fineness ratio, ℓ/d, to the 1/4 power for fineness ratios between 1/6 and 1. For fineness ratios greater than 1, the power increased and approached unity, as would be expected from shaped-charge jet theory. For engineering purposes, in the hypervelocity regime, a sphere produces the same crater as a cylinder of equal diameter and ℓ/d of 2/3.

INTRODUCTION

The crater resulting from a projectile impacting a semi-infinitely thick target depends primarily on: the projectile diameter, density, and shape; the target density and strength; the velocity of the projectile at impact; and the angle between the flight path and the target face.

All of these factors have been studied experimentally, particularly the effects of velocity, quite naturally. References 1 through 6 are examples of the experimental treatment of the influence of these factors on cratering.

The effects of projectile shape have received very little attention. Theoretical studies have usually concerned a cylindrical projectile with its length equal to its diameter, and the application of the results even to cylinders of other fineness ratios is uncertain. Experimentally, it is sometimes very difficult, if not impossible, to launch any but very short projectiles at very high velocities, so that most of the available results are for cylinders with fineness ratios less than 1, or for spheres.

It has been theorized (see, e.g., refs. 7 and 8) that the crater volume should be proportional to projectile energy, and hence (for a given velocity) to the projectile mass. Therefore, for geometrically similar craters, the penetration depth would vary as the cube root of the projectile mass. Under this rule, the ratio of penetration depth to projectile diameter varies as the projectile fineness ratio to the 1/3 power (for a given projectile density).

To investigate the validity of this hypothesis, an experimental investigation was undertaken to determine the effect of cylinder fineness ratio and projectile shape on the various crater parameters (penetration, diameter, shape, and volume) for impacts in thick hard-aluminum targets up to velocities of 11.3 km/sec. Projectiles were linear, high-density, polyethylene cylinders and spheres. The cylinder fineness ratios were 1/6, 1/3, 2/3, 1, and 3.

SYMBOLS

D diameter of crater measured in plane of undisturbed surface, mm

d projectile diameter, mm

l length of projectile, mm

m mass of projectile, gm

P penetration (maximum depth of crater) measured from undisturbed surface, mm

U crater volume measured from undisturbed surface, cm^3

U_p projectile volume, cm^3

v velocity of projectile at impact, km/sec

EXPERIMENTAL PROCEDURE

The 5- to 6-mm projectiles used in this experiment (table I) were launched into free flight by light-gas guns. It was necessary to support the 1/6-caliber cylinders and the spheres in sabots in order to maintain structural integrity during launch. Other projectiles were launched without sabots; their diameters matched the gun bore at the time of launch.

The targets were made of 2024-T351 aluminum, with a Brinell hardness of nominally 120. Target thickness and width were at least four times the penetration depth and crater diameter, respectively.

The ballistic range used is described in reference 9. It has six spark shadowgraph stations, each presenting two orthogonal views of the projectile in flight. Two stations were equipped with Kerr-cell shutters with exposure times of about 5 nsec, so that the structural integrity of the model could be ascertained. The six stations provided a position time history of the projectile's flight and it was determined from these records that 56 percent of the cylinders impacted the target at approximately 0° angle of attack, 90 percent

at angles of 5° or less, and 10 percent at angles greater than 5°. The maximum angle at impact was about 10°. A scrutiny of the data revealed that any anomalies due to angle of impact were outweighed by the inherent variation in crater formation.

All crater dimensions were measured with the undisturbed target face as the reference plane. Penetration depths were measured with a specially adapted dial indicator. Crater diameters were measured with a filar-micrometer microscope. (Four readings from edge to edge of the damaged area were made, then averaged to give the diameter.) Crater volumes were measured with a micrometer buret using a liquid composed of water and a wetting agent.

DISCUSSION OF RESULTS

A compilation of the pertinent data resulting from this investigation can be found in table I.

These data were analyzed by the technique employed in reference 1. Consider the four basic nondimensional crater parameters: penetration, P/d; diameter, D/d; shape, P/D; volume, U/U_p. The volume of craters with similar profiles may be expressed as

$$U \sim PD^2 \tag{1}$$

The projectile volume is

$$U_p \sim d^2 l$$

Thus

$$U/U_p \sim PD^2/d^2 l \tag{2}$$

but

$$PD^2/d^2 l = (P/d)^2 (D/d)(D/P)(d/l) \tag{3}$$

and so

$$U/U_p = \text{const.}\ (P/d)^2 (D/d)(D/P)(d/l) \tag{4}$$

where the dimensionless parameters, P/d, D/d, and D/P are expressed as functions of the projectile fineness ratio, l/d, and the impact velocity, v. With all four crater parameters in a single equation, best fits to the penetration, diameter, shape, and volume data were simultaneously acquired, graphically, to satisfy equation (4) (figs. 1 through 4).

Nondimensional penetration as a function of impact velocity is shown in figure 1. This set of data was used to determine the transition point to the hypervelocity regime for each shape. The transition velocities are marked by

ticks on the individual sets of data. Only those data above the transition point were considered in determining the effects of projectile shape on impact. The velocity at which transition occurs decreases with increasing fineness ratio. The data for spherical projectiles show a transition point lower than their counterpart ($\ell/d = 2/3$) and deeper penetrations at lower speeds.

The nondimensional crater diameter, shape, and volume parameters are shown as functions of the impact velocity in figures 2, 3, and 4, respectively. Crater diameter is also plotted in the more usual Cartesian form in figure 2(b).

The fit to the data is illustrated in figure 5, where each parameter is plotted as a function of the fineness ratio. The following points are to be noted from this figure: (1) the ratio of crater diameter to projectile diameter tends to become constant at very high fineness ratios, a characteristic found by Nysmith and Denardo (ref. 10), although not stated in these terms; (2) the penetration depth approaches a linear relationship with projectile length at a fineness ratio of 3; and (3) although the power law found for the other three parameters deviates beyond a fineness ratio of 1, the law for crater volume applies to at least a fineness ratio of 3.

Equations defining each crater parameter are given below for the hypervelocity impact regime:

$$P/d = 0.34\ (\ell/d)^{1/4}(v)^{2/3} \tag{5}$$

$$D/d = 1.53\ (\ell/d)^{1/2}(v)^{1/2} \tag{6}$$

$$P/D = 0.22\ (\ell/d)^{-1/4}(v)^{1/6} \tag{7}$$

$$U/U_p = 0.36\ (\ell/d)^{1/4}(v)^{5/3} \tag{8}$$

Profiles of typical craters formed by the hypervelocity impact of the various projectiles (fig. 6) clearly illustrate a significant change in crater shape with fineness ratio. (The customary raised lips associated with high velocity impact are not seen in figures 6 and 7. It was necessary to remove the raised portion of the target faces prior to sectioning in order to measure the diameter and volume of the crater.)

An unusual cratering process was noted in the fineness ratio 1/6 tests. Three distinct crater profiles were found in various parts of the velocity range. As shown in figure 7, at low speeds, below 4 km/sec, a rather shallow and very smooth crater containing a small indentation was formed. (Note subsurface cavity directly beneath indentation.) Between 4.5 and 7 km/sec, the small indentation grew to a rough-surfaced conical cavity with the remainder of the crater surface being smooth. Above 7 km/sec, the crater was conical shaped with a rough surface finish similar to those produced by cylinders with fineness ratios of 1/3.

The technique of data fitting applied in the hypervelocity regime was attempted at lower speeds. Unfortunately, no correlation was found, due to an inconsistency or lack of data for some of the projectile shapes tested.

CONCLUDING REMARKS

The ratio of penetration depth to projectile diameter has been found to vary with the projectile fineness ratio to the 1/4 power for polyethylene projectiles impacting thick, hard aluminum targets in the hypervelocity impact regime. This result differs from the commonly assumed value of 1/3, which is the result of the assumption that the penetration is a function of the cube root of the projectile mass. One reason for this deviation is that crater shape varies significantly with the fineness ratio of the projectile.

The effects of projectile shape on the cratering parameters follows a power law for fineness ratios between 1/6 and 1; the power deviates for fineness ratios above 1. In the case of the crater volume, however, the power law exponent remains constant up to the highest fineness ratio tested ($l/d = 3$).

Spheres produce craters similar to those made by cylinders (of the same diameter and material) with fineness ratios of 2/3, in the hypervelocity impact regime.

Ames Research Center
National Aeronautics and Space Administration
Moffett Field, Calif., 94035, Sept. 11, 1968
124-09-15-02-00-21

REFERENCES

1. Denardo, B. Pat; Summers, James L.; and Nysmith, C. Robert: Projectile Size Effects on Hypervelocity Impact Craters in Aluminum. NASA TN D-4067, 1967.

2. Summers, James L.: Investigation of High-Speed Impact: Regions of Impact and Impact at Oblique Angles. NASA TN D-94, 1959.

3. Denardo, B. Pat: Penetration of Polyethylene Into Semi-infinite 2024-T351 Aluminum Up to Velocities of 37,000 Feet per Second. NASA TN D-3369, 1966.

4. Fish, Richard H.: The Penetration of Porous Projectiles in Aluminum and Plastic Targets. NASA TN D-4505, 1968.

5. Gehring, J. W.; and Wenzel, A. B.: Hypervelocity Impact Studies Against Apollo-Type Structures Up to 16.5 Km/Sec. Final Report, P.O. No. M458XA-406033, NAA General Motors Defense Res. Labs. Rep., TR65-56, July 1965.

6. Piacesi, R.; Waser, R. H.; and Dawson, V. C. D.: Determination of the Yield Strength as an Effective Mechanical Strength Property in the Cratering Process of Hypervelocity Impact. Seventh Hypervelocity Impact Symposium, Proc., vol. V, Feb. 1965, pp. 259-271.

7. Walsh, J. M.; Johnson, W. E.; Dienes, J. K.; Tillotson, J. H.; and Yates, D. R.: Summary Report on the Theory of Hypervelocity Impact. GA-5119, General Atomic, Division of General Dynamics, March 1964.

8. Heyda, J. F.; and Riney, T. D.: Peak Axial Pressures in Semi-infinite Media Under Hypervelocity Impact. Seventh Hypervelocity Impact Symposium, Proc., vol. III, Feb. 1965, pp. 75-122.

9. Nysmith, C. Robert: Penetration Resistance of Double-Sheet Structures at Velocities to 8.8 Km/Sec. NASA TN D-4568, 1968.

10. Nysmith, C. Robert; and Denardo, B. Pat: Investigation of the Impact of High-Fineness-Ratio Projectiles Into Thick Targets. NASA TN D-3304, 1966.

TABLE I.- SUMMARY OF PERTINENT DATA

Round	Projectile shape	m, gm	d, mm	ℓ, mm	P, mm	D, mm	U, cm^3	v, km/sec
1076	1/6-	0.0154	5.083	0.848	3.71	9.47	0.082	6.986
1079	caliber	.0164	5.098	.853	4.04	8.94	.111	7.673
1084	cylinder	.0164	5.083	.856	4.32	10.3	.136	8.344
1085	↓	.0155	5.083	.831	4.45	9.45	.129	8.478
1087		.0162	5.083	.833	4.75	9.91	.153	9.091
1088		.0165	5.083	.853	3.76	8.43	.083	6.721
1089		.0160	5.080	.836	3.23	7.92	.069	6.088
1090		.0164	5.080	.859	3.00	7.65	.072	5.724
1091		.0166	5.083	.856	3.30	8.05	.070	5.968
1092		.0168	5.083	.856	2.34	7.19	.045	4.614
1093		.0167	5.083	.856	2.46	7.16	.050	4.557
1095		.0164	5.083	.853	.79	6.55	.023	3.173
1096		.0163	5.083	.848	.91	6.65	.025	3.650
1097		.0158	5.083	.841	4.72	9.93	.159	9.231
1105	↓	.0161	5.083	.841	5.03	9.91	.189	9.755
566	1/3-	.0457	5.639	1.880	7.21	16.9	.692	10.587
567	caliber	.0438	5.690	1.829	7.19	16.1	.624	10.826
568	cylinder	.0453	5.702	1.803	7.54	17.0	.790	11.295
581	↓	.0427	5.664	1.803	6.63	14.9	.515	9.597
583		.0414	5.537	1.803	5.66	13.4	.370	7.775
587		.0431	5.664	1.803	4.78	12.2	.226	6.741
588	↓	.0438	5.677	1.803	4.39	11.9	.210	6.395
150	2/3-	.0989	5.860	3.889	6.73	20.7	1.082	7.882
708	caliber	.0968	5.779	3.886	7.65	22.2	1.410	9.296
1049	cylinder	.0874	5.591	3.741	7.16	21.1	1.110	8.903
SP-785	↓	.1061	6.071	4.064	6.10	18.3	.761	6.770
SP-861		.1019	5.867	4.013	2.92	12.6	.178	3.712
SP-863		.1045	5.906	4.013	4.75	16.9	.468	5.741
SP-868		.1023	5.880	4.013	3.66	15.0	.291	4.587
SP-905	↓	.1051	5.969	4.013	7.09	21.8	1.250	8.498
137	1-caliber	.1487	5.855	5.855	6.30	22.1	1.115	6.291
139	cylinder	.1504	5.860	5.931	6.91	22.1	1.371	6.754
140	↓	.1499	5.857	5.880	6.96	23.2	1.368	6.922
143		.1499	5.852	5.931	7.14	22.4	1.407	6.951
144		.1512	5.852	5.933	7.42	24.0	1.547	7.283
146		.1500	5.860	5.875	6.07	21.6	1.109	6.244
147		.1490	5.867	5.842	5.82	21.3	.977	5.941
148		.1496	5.867	5.872	4.95	20.0	.772	5.125
153		.1501	5.867	5.893	6.96	23.5	1.414	6.867
155		.1506	5.880	5.885	4.65	19.0	.665	4.770
704		.1299	5.563	5.613	7.59	23.7	1.479	7.980
710		.1510	5.870	5.842	8.31	24.8	1.921	8.458
1051		.1372	5.692	5.697	8.18	26.2	1.903	8.441
1108	↓	.1527	5.900	5.895	8.74	26.2	2.176	8.780
142	3-caliber	.4487	5.855	17.49	11.8	29.1	3.452	4.955
145	cylinder	.4489	5.855	17.60	11.9	27.4	3.562	5.195
149	↓	.4515	5.867	17.59	10.0	22.8	2.323	4.366
151		.4501	5.867	17.54	9.02	21.7	1.814	3.840
152		.4490	5.857	17.58	12.4	28.9	3.870	5.404
1047	↓	.5292	6.200	18.59	13.4	31.5	4.770	5.765
1058	sphere	.0659	5.077	5.077	4.67	15.8	.457	6.046
1059	↓	.0661	5.085	5.085	4.52	16.1	.428	5.745
1065		.0669	5.085	5.085	3.96	14.9	.316	5.102
1066		.0674	5.100	5.100	3.48	13.6	.225	4.526
1067		.0666	5.083	5.083	3.18	12.8	.187	4.180
1068		.0662	5.085	5.085	2.97	12.2	.126	3.932
1071		.0663	5.060	5.060	5.36	18.0	.601	7.148
1072		.0665	5.067	5.067	5.00	16.3	.459	6.404
1075		.0663	5.062	5.062	5.84	18.2	.639	7.532
1099		.0662	5.062	5.062	5.46	17.8	.617	7.314
1100		.0665	5.070	5.070	5.69	18.3	.704	7.728
1101		.0664	5.067	5.067	5.74	18.7	.735	7.887
1103		.0665	5.070	5.070	5.26	17.2	.566	6.904
1106	↓	.0666	5.083	5.083	5.99	18.6	.753	8.252

Page Intentionally Left Blank

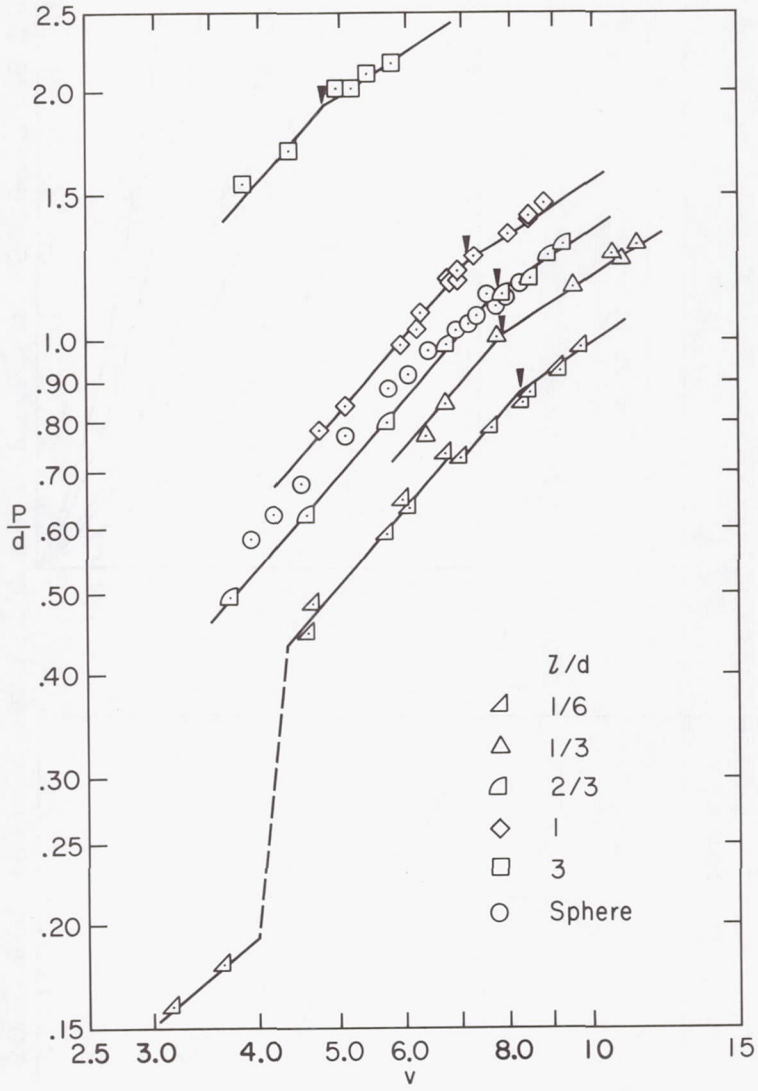

Figure 1.- Penetration as a function of velocity.

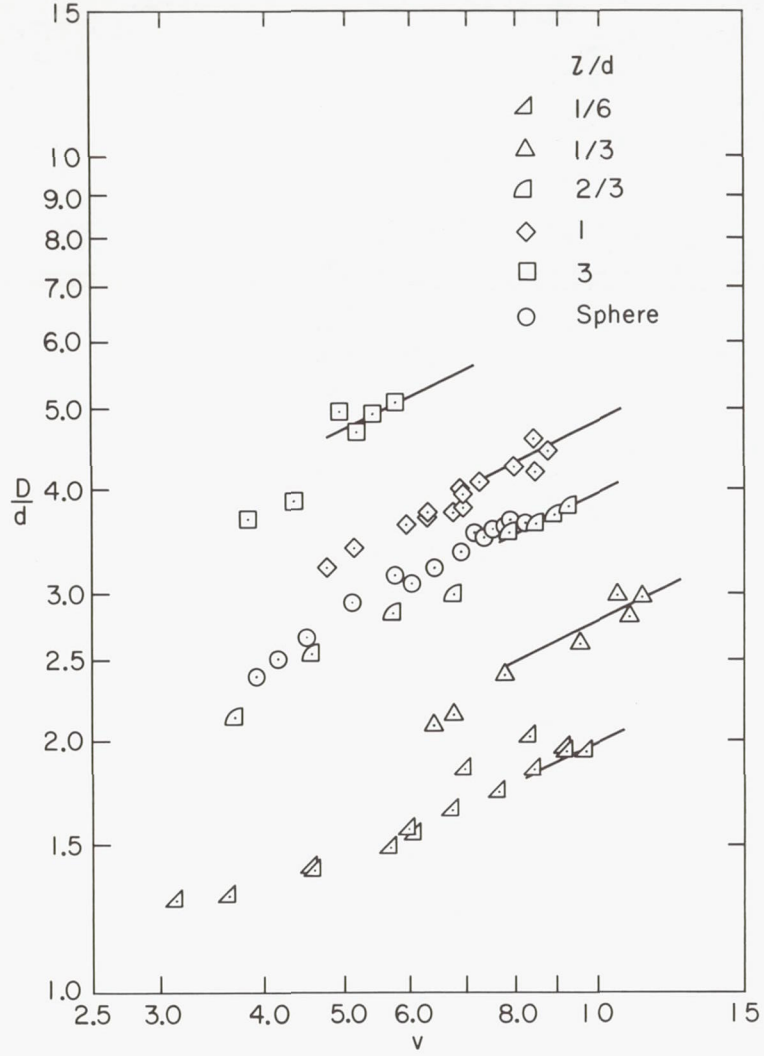

(a) Log-log plot.

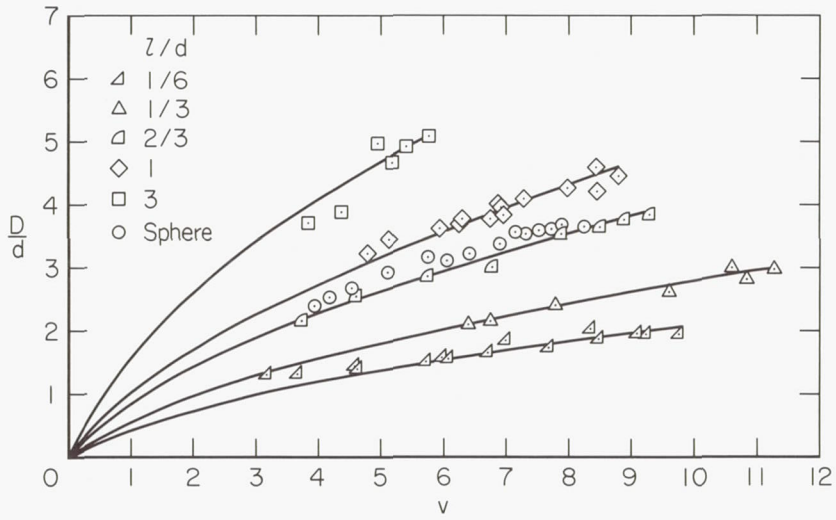

(b) Cartesian plot.

Figure 2.- Diameter as a function of velocity.

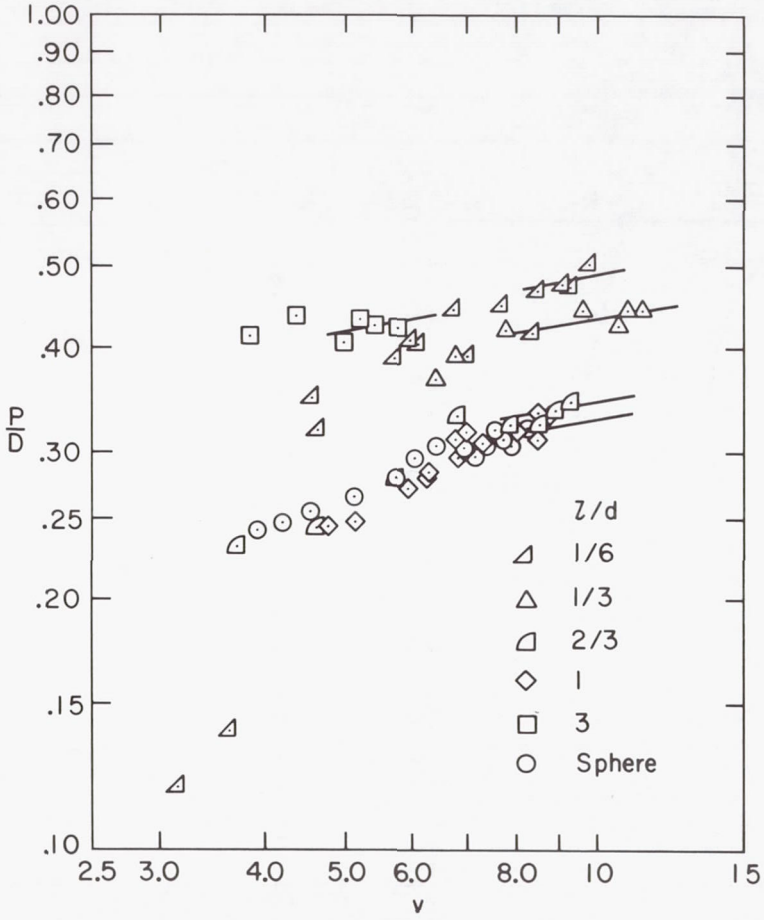

Figure 3.- Crater shape as a function of velocity.

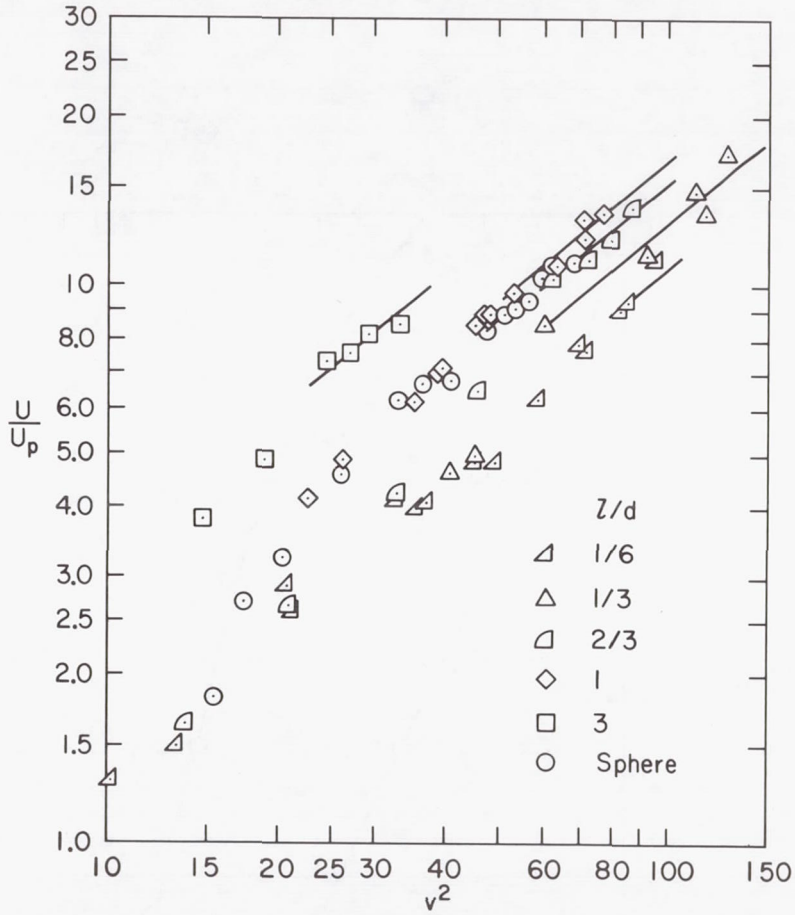

Figure 4.- Volume as a function of velocity squared.

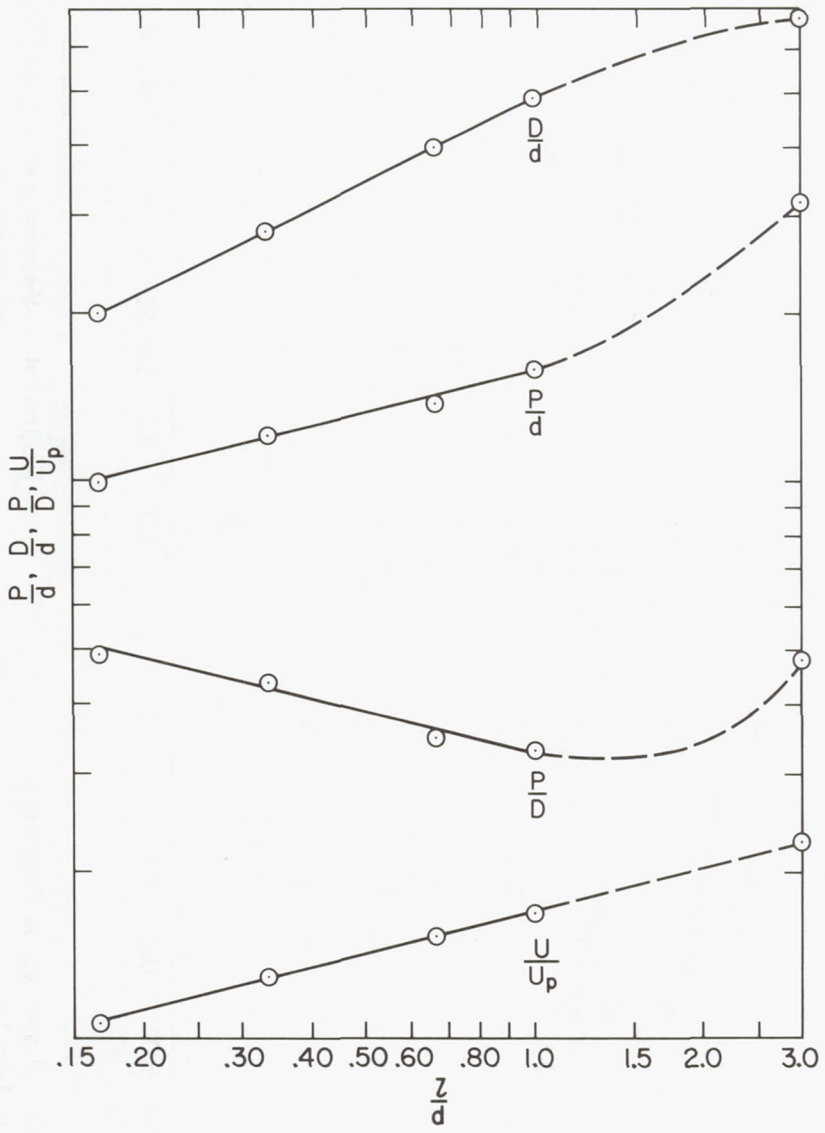

Figure 5.- Parametric analysis data fits.

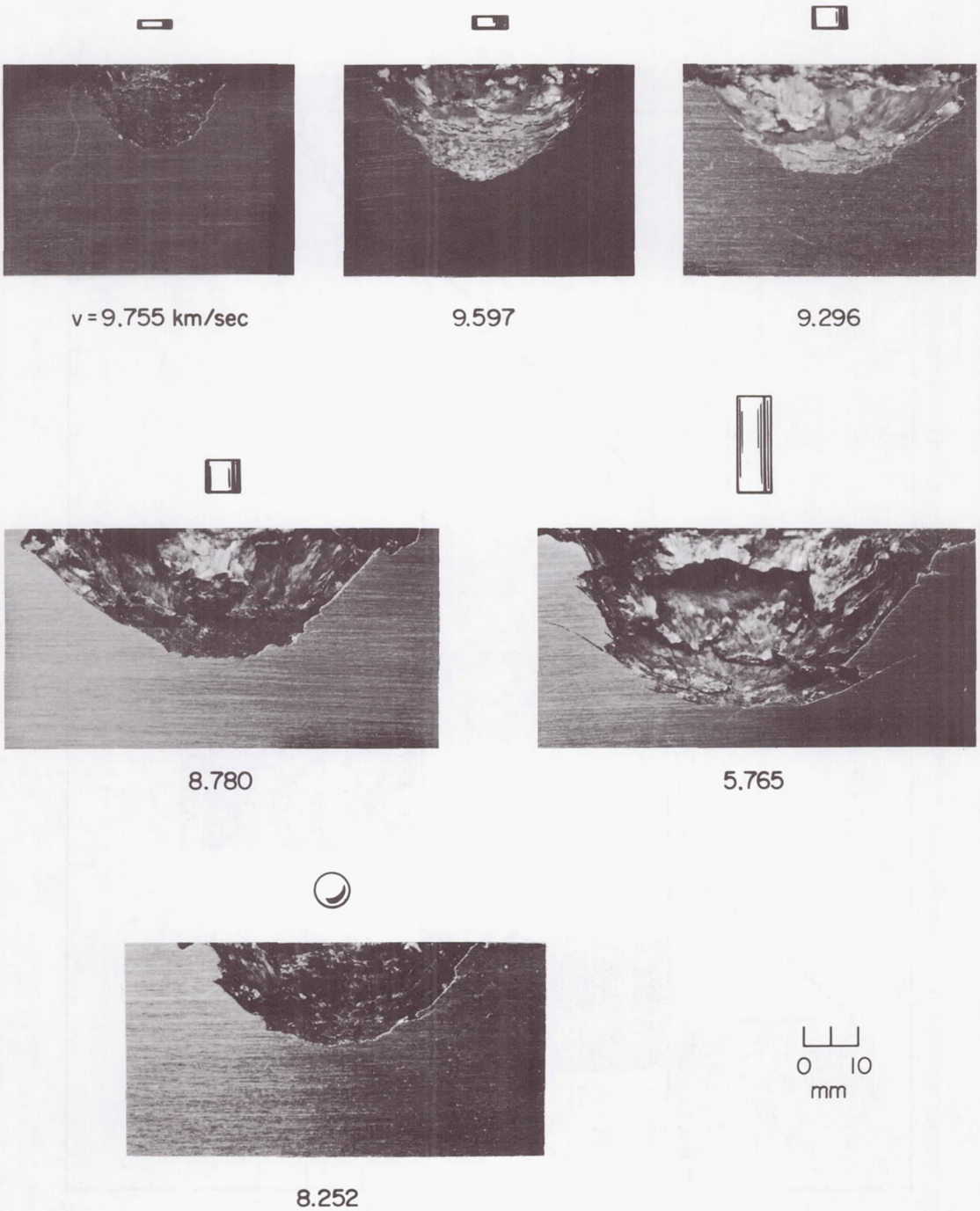

Figure 6.- Typical impact craters in the hypervelocity regime for various projectile shapes.

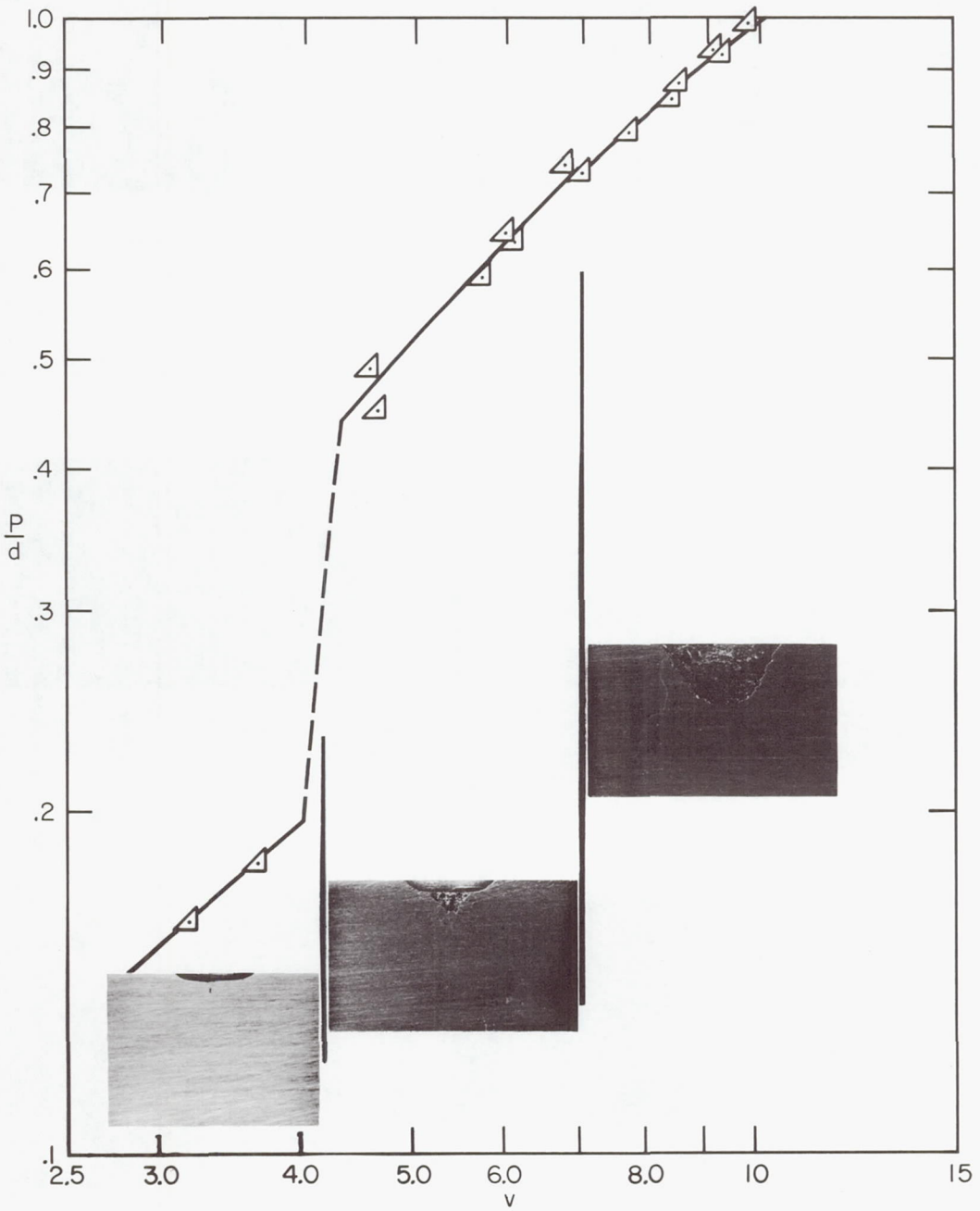

Figure 7.- Cratering regimes for impacts with $\ell/d = 1/6$ cylinder.

NASA-Langley, 1968 —— 32 A-3061